ATOMIC CLOCKS AND ATOM INTERFEROMETRY

CHRISTIAN J. BORDÉ
Laboratoire de Physique des Lasers
UMR 7538 CNRS, Université Paris-Nord
99, Avenue J.-B. Clément, 93430, Villetaneuse, France
and
ERGA/LERMA, UMR 8540 CNRS, Université Paris VI
4 Place Jussieu, 75005 Paris, France

Abstract. We show that the language of atom interferometry [1] provides a unified picture for microwave and optical atomic clocks as well as for gravito-inertial sensors. The sensitivity and accuracy of these devices, is now such that a new theoretical framework [2] common to all these interferometers, is required and which includes: 1 - A fully quantum mechanical treatment of the atomic motion in free space and in the presence of a gravitational field (most cold atom interferometric devices use atoms in "free fall" in a fountain geometry), 2 - An account of simultaneous actions of gravitational and electromagnetic fields in the interaction zones, 3 - A second quantization of the matter fields to take into account their fermionic or bosonic character in order to discuss the role of coherent sources and their noise properties, 4 - A covariant treatment including spin to evaluate general relativistic effects. A theoretical description of atomic clocks revisited along these lines, is presented, using both an exact propagator of atom waves in gravito-inertial fields [3] and a covariant Dirac equation in the presence of weak gravitational fields [4]. Using this framework, recoil effects, spin-related effects, beam curvature effects, the sensitivity to gravito-inertial fields and the influence of the coherence of the atom source can be discussed in the context of present and future atomic clocks and gravito-inertial sensors.

1. Introduction

The first purpose of these few pages is to clarify the link between atomic clocks and the recent field of atom interferometry [1] and to show that

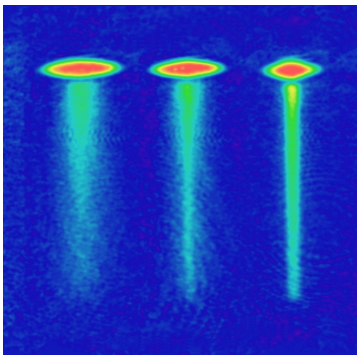

Figure 1. Rubidium atoms are extracted from a cold Rubidium gas (left) and from a Bose-Einstein condensate (right). *(Courtesy of the University of Munich [7])*

indeed, microwave and optical atomic clocks are genuine atom interferometers [2]. The wave character of atoms is getting more and more manifest in these devices: the recoil energy $\hbar\delta = \hbar^2 k^2/2M$ is not negligible any more in Cesium clocks ($\delta/2\pi\nu \simeq 1.5\ 10^{-16}$). Atom sources may now be coherent sources of matter-waves (Bose-Einstein condensates [6, 7], atom lasers or atomasers [8]) as illustrated in Fig. 1. We have to deal with a very different picture from that of small clocks carried by classical point particles. The atomic frame of reference may not be well-defined. In modern microwave atomic clocks (see Fig. 2) atoms interact twice with an electromagnetic field (this is the method of separated fields introduced by N. F. Ramsey around 1950) giving rise to interference fringes (Fig. 3), which can now be reinterpreted as an interference between the de Broglie waves associated with the external motion of the atoms. Atomic clocks are thus now fully quantum devices in which both the internal and external degrees of freedom must be quantized.

Gravitation and inertia play a key role in slow atom clocks. The Einstein red shift and the second-order Doppler shift may become important and thus atomic clocks have to be treated also as relativistic devices.

Finally, we recall how the idea of separated e.m. fields in space or time has been extended to the optical domain in order to build atom interferometers, which can be used as optical clocks, but also as very sensitive gravito-inertial sensors.

2. Atom waves

The wave properties of atoms are fully described by a dispersion law relating the de Broglie frequency to the de Broglie wave vector, which is obtained

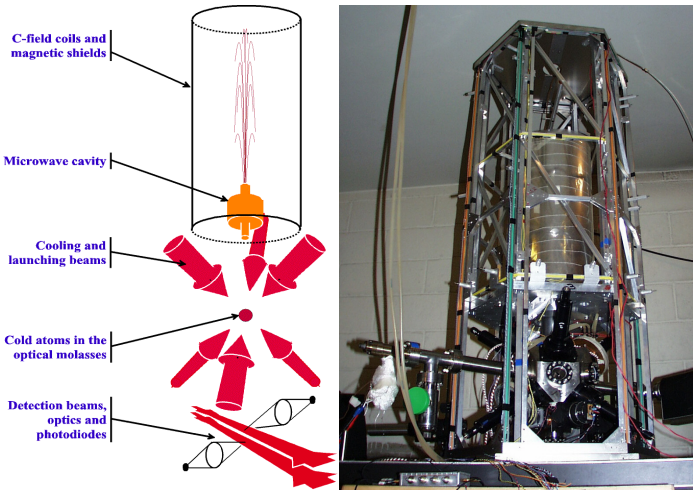

Figure 2. Principle and realization of a fountain clock (*courtesy of BNM-LPTF[5]*)

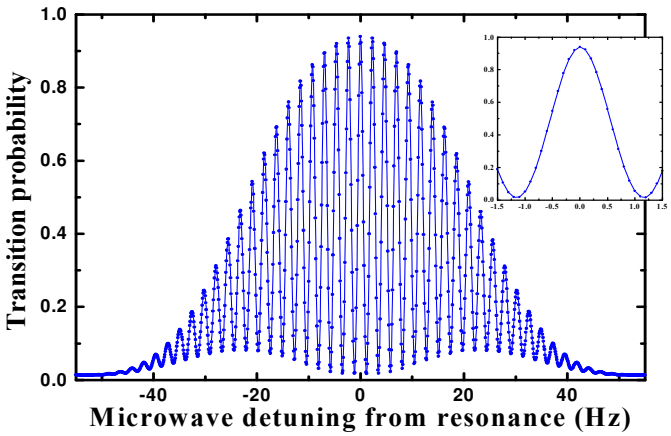

Figure 3. Ramsey fringes obtained with the Cesium fountain clock (*Courtesy of BNM-LPTF[5]*)

from the law connecting the energy $E(\overrightarrow{p})$ to the momentum $\overrightarrow{p}$ by the introduction of Planck constant. In free space (Fig. 4) the corresponding

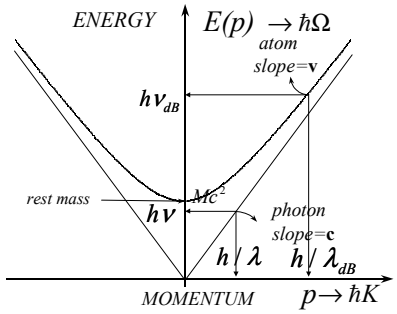

Figure 4. Energy-momentum curves: (1D cut of the mass shell) hyperbola for a massive particle e.g. an atom in a given internal energy state and straight lines for photons. The slope is the group velocity of the de Broglie wave.

curve is the hyperbola of equation:

$$E(\overrightarrow{p}) = \sqrt{M^2c^4 + p^2c^2} \tag{1}$$

The amplitude of an atom wave may therefore be written generally as:

$$\begin{aligned} a(\overrightarrow{r},t) &= \int dE \frac{d^3p}{(2\pi\hbar)^{3/2}} e^{i[\overrightarrow{p}\cdot(\overrightarrow{r}-\overrightarrow{r}_0)-E(t-t_0)]/\hbar} \\ &\quad \delta\left(E^2 - E^2(\overrightarrow{p})\right)\theta(E)\, a(\overrightarrow{p},E) \\ &= \int \frac{dE}{2E(\overrightarrow{p})} \frac{d^3p}{(2\pi\hbar)^{3/2}} e^{i[\overrightarrow{p}\cdot(\overrightarrow{r}-\overrightarrow{r}_0)-E(t-t_0)]/\hbar} \\ &\quad \delta\left(E - E(\overrightarrow{p})\right) a(\overrightarrow{p},E) \end{aligned} \tag{2}$$

In the non-relativistic limit:

$$a(\overrightarrow{r},t) = \int \frac{d^3p}{(2\pi\hbar)^{3/2}} e^{i\left[\overrightarrow{p}\cdot(\overrightarrow{r}-\overrightarrow{r}_0)-\left(Mc^2+p^2/2M\right)(t-t_0)\right]/\hbar} a(\overrightarrow{p}) \tag{3}$$

If $a(\overrightarrow{p})$ is expanded, for example, in Hermite-Gauss functions,

$$\begin{aligned} a(p_x,p_y,p_z) &= \frac{1}{(2\pi)^{3/2}\sqrt{\Delta_x\Delta_y\Delta_z}} \sum_{lmn} H_l\left(\frac{p_x}{\Delta_x}\right) H_m\left(\frac{p_y}{\Delta_y}\right) H_n\left(\frac{p_z}{\Delta_z}\right) \\ &\quad \exp\left[-\frac{p_x^2}{2\Delta_x^2}\right] \exp\left[-\frac{p_y^2}{2\Delta_y^2}\right] \exp\left[-\frac{p_z^2}{2\Delta_z^2}\right] \end{aligned} \tag{4}$$

we obtain a complete orthogonal set of free-propagation modes. The lowest order modes correspond to minimum uncertainty wave packets. These

free-space propagation modes transform with the same ABCD law as in Gaussian laser optics. The ABCD matrices are functions of time in this case and we shall see below how the ABCD law can be generalized in the presence of gravito-inertial fields. For a travelling wave the δ function can be written $\delta\left(p_x - \sqrt{2ME_{kin} - p_y^2 - p_z^2}\right)$ and we may keep the kinetic energy $E_{kin} = E - Mc^2$ instead of p_x in the expression of the modes. This is a good choice if the atom wave is monochromatic, in which case the integral over energy combines with an amplitude proportional to $\delta\left(E_{kin} - E_0\right)$. In the paraxial approximation $\delta\left(p_x - \sqrt{2ME_{kin} - p_y^2 - p_z^2}\right)$ goes into $\delta\left(p_x - \sqrt{2ME_{kin}}\left(1 - \left(p_y^2 + p_z^2\right)/\left(4ME_{kin}\right)\right)\right)$ and

$$a(\overrightarrow{r},t) \propto \int dp_y dp_z a(p_y,p_z) \exp\left[-\frac{i}{\hbar}\frac{p_y^2+p_z^2}{2\sqrt{2ME_0}}(x-x_0) + \frac{i}{\hbar}(p_y y + p_z z)\right] \exp\left[\frac{i}{\hbar}\sqrt{2ME_0}(x-x_0) - \frac{i}{\hbar}\left(Mc^2+E_0\right)(t-t_0)\right] \quad (5)$$

The same Hermite-Gauss expansion as above may be used for $a(p_y, p_z)$. Again the propagation is described by ABCD matrices, which are in this case functions of x.

3. Interaction of two-level atoms with electromagnetic waves

We shall make a systematic use of energy-momentum diagrams to discuss the problem of interaction of two-level atoms with two separated field zones in a Ramsey excitation scheme (Figure 5).

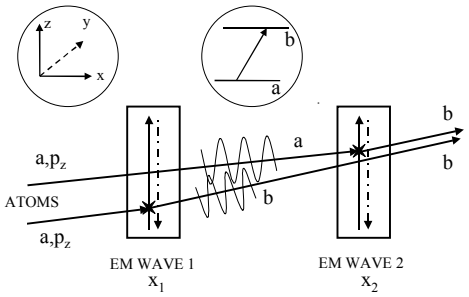

Figure 5. Illustration of the reinterpretation of the separated field method as the interference between de Broglie waves. Case of successive interactions with copropagating waves.

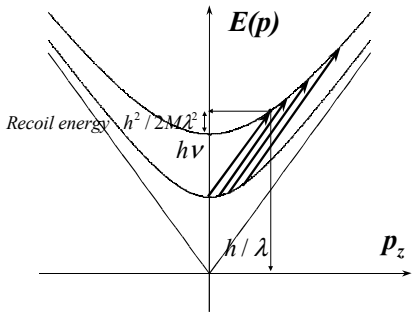

Figure 6. Energy vs transverse momentum in the absorption of a photon by a two-level atom. A distribution of absorbed frequencies correspond to a distribution of momenta.

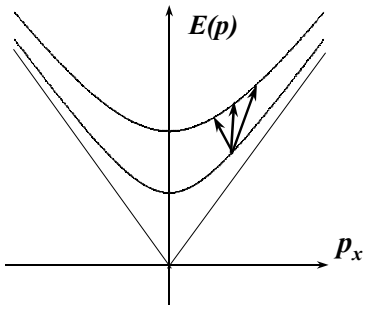

Figure 7. Energy vs longitudinal momentum in the absorption of a photon by a two-level atom. When the e.m. is confined in the longitudinal direction, there is a corresponding distribution of wave vector components in that direction, which allows for a spread of absorbed frequencies (transit-time broadening or Rabi pedestal) and a change of the longitudinal momentum of the atom.

Figures 6 and 7 illustrate the energy and momentum conservation between this two-level atom and effective photons from each travelling wave in the transverse and longitudinal directions and display the recoil energy, the first and second-order Doppler shifts and the transit broadening. It is clear from Fig. 7 that, out of resonance, an additional longitudinal momentum is transferred to the atoms in the excited state. This velocity change along the forward direction is the basis for the so-called mechanical reinterpretation of Ramsey fringes [9, 10, 11, 12, 13]. We will now illustrate this point in more detail through a simple first-order theory of Ramsey fringes.

Let us consider a beam of two-level atoms with $\mathrm{E}_a < \mathrm{E}_b$ initially in state a which interacts successively with two field zones respectively centered at x_1 and x_2 as in Fig. 5 and let us calculate the excited state amplitude

to first order in each field zone [2, 3]. One can check that the following expression is indeed a first-order solution of Schroedinger equation:

$$\begin{aligned} b^{(1)}(\overrightarrow{r},t) &= \frac{1}{i\hbar}\int_{-\infty}^{t}dt'\int\frac{d^3p}{(2\pi\hbar)^{3/2}}\int\frac{d^3k}{(2\pi)^{3/2}}V_{ba}(\overrightarrow{k},t')e^{i\overrightarrow{k}\cdot(\overrightarrow{r}-\overrightarrow{r_1})} \\ & e^{i\left[E_b(\overrightarrow{p}+\hbar\overrightarrow{k})-E_a(\overrightarrow{p})\right](t'-t)/\hbar} \\ & e^{i[\overrightarrow{p}\cdot(\overrightarrow{r}-\overrightarrow{r}_0)-E_a(\overrightarrow{p})(t-t_0)]/\hbar}\langle a|\langle\overrightarrow{p}|\Psi^{(0)}\rangle \end{aligned} \tag{6}$$

where the energy is given by the dispersion relation 1 and can be expanded in a Taylor series:

$$E(\overrightarrow{p}+\hbar\overrightarrow{k})=E(\overrightarrow{p})+\frac{\hbar\overrightarrow{k}\cdot\overrightarrow{p}c^2}{E(\overrightarrow{p})}+\frac{(\hbar k)^2c^2}{2E(\overrightarrow{p})}+...=E(\overrightarrow{p})+\hbar\overrightarrow{k}\cdot\overrightarrow{v}+\frac{(\hbar k)^2}{2M}+... \tag{7}$$

The matrix element of the Hamiltonian of interaction with the e.m. waves is $V_{ba}(\overrightarrow{r},t)=-\Omega_{ba}e^{i(\pm kz-\omega t+\varphi)}U(\overrightarrow{r})$, where Ω_{ba} is a Rabi frequency. Let us introduce a monochromatic electromagnetic wave with a Gaussian distribution of k_x (example for the illustration) and, for simplicity, let us ignore the dimension y :

$$\begin{aligned} b_{\pm}^{(1)}(\overrightarrow{r},t) &= i\Omega_{ba}e^{i(\pm kz-\omega t+\varphi)}\frac{w}{2\sqrt{\pi}}\int\frac{d^3p}{(2\pi\hbar)^{3/2}} \\ & \int_{-\infty}^{+\infty}dk_x e^{-\frac{w^2k_x^2}{4}}e^{ik_x(x-x_1)}e^{i[\omega-\omega_{ba}\mp kv_z-k_xv_x-\delta](t-t_1)} \\ & \int_{-\infty}^{t}dt'e^{-i[\omega-\omega_{ba}\mp kv_z-k_xv_x-\delta](t'-t_1)} \\ & e^{i[\overrightarrow{p}\cdot(\overrightarrow{r}-\overrightarrow{r}_0)-E_a(\overrightarrow{p})(t-t_0)]/\hbar}a^{(0)}(\overrightarrow{p}) \end{aligned} \tag{8}$$

with $\hbar\omega_{ba}(\overrightarrow{p})=E_b(\overrightarrow{p})-E_a(\overrightarrow{p})\approx\hbar\omega_{ba}\sqrt{1-v^2/c^2}=\hbar\omega_{ba}(v)$ and $a^{(0)}(\overrightarrow{p})=\langle a|\langle\overrightarrow{p}|\Psi^{(0)}\rangle$. In the time integral the upper bound t may be extended to infinity if the considered wave packet has left the interaction zone (this is justified in the footnote [1], where the exact calculation of reference

[1]The exact calculation gives:

$$\begin{aligned} b_{\pm}^{(1)}(\overrightarrow{r},t) &= i\frac{\sqrt{\pi}w\Omega_{ba}}{2}e^{i(\pm kz-\omega t+\varphi)}\int\frac{d^3p}{(2\pi\hbar)^{3/2}}\frac{1}{v_x} \\ & \Big[2e^{-w^2(\omega-\omega_{ba}\mp kv_z-\delta)^2/4v_x^2}e^{i(\omega-\omega_{ba}\mp kv_z-\delta)(x-x_1)/v_x} \\ & -w(i\rho)\Big]e^{i[\overrightarrow{p}\cdot(\overrightarrow{r}-\overrightarrow{r}_0)-E_a(\overrightarrow{p})(t-t_0)]/\hbar}a^{(0)}(\overrightarrow{p}) \end{aligned} \tag{9}$$

with $\rho=(x-x_1)/w_0+i(\omega-\omega_{ba}\mp kv_z-\delta)w_0/2v_x$ and where $w(z)$ is the error function of complex arguments. The second term vanishes with the distance $(x-x_1)/w_0$ leaving the accelerated or decelerated first contribution as the dominant one.

[12] is recalled). We obtain a δ function expressing energy conservation as expected from the S-matrix:

$$2\pi\delta(\omega - \omega_{ba}(v) \mp kv_z - k_x v_x - \delta)$$

and corresponding to Figures 6 and 7. If the resonance condition $\omega - \omega_{ba}(v) \mp kv_z - \delta = 0$ is satisfied in Fig. 6 this implies $k_x = 0$ in Fig. 7, otherwise the effect of energy conservation is to select a particular component $k_x = (\omega - \omega_{ba}(v) - kv_z - \delta)/v_x$.

We obtain the first-order excited state transition amplitude:

$$\begin{aligned} b_{\pm}^{(1)}(\overrightarrow{r},t) &= i\sqrt{\pi}e^{i(\pm kz-\omega t+\varphi)}\int \frac{d^3p}{(2\pi\hbar)^{3/2}}\frac{w\Omega_{ba}}{v_x}e^{-w^2(\omega-\omega_{ba}\mp kv_z-\delta)^2/4v_x^2} \\ &\quad e^{i(\omega-\omega_{ba}\mp kv_z-\delta)(x-x_1)/v_x}e^{i[\overrightarrow{p}\cdot(\overrightarrow{r}-\overrightarrow{r}_0)-E_a(\overrightarrow{p})(t-t_0)]/\hbar}a^{(0)}(\overrightarrow{p}) \end{aligned} \tag{10}$$

as the product of the e.m. carrier times a Rabi frequency and a Rabi envelope, times an additional momentum phase factor for each initial wave packet Fourier component. This additional longitudinal momentum is proportional to the detuning and is responsible for the Ramsey fringes, since de Broglie waves associated with each path have a different wavelength in the dark zone (Fig. 5) and the transition probability integrated over the detection volume is:

$$\begin{aligned} \int d^3r\ b_{1\pm}^{(1)}(\overrightarrow{r},t)b_{2\pm}^{(1)*}(\overrightarrow{r},t) &\propto \int dp_z e^{-w^2(\omega-\omega_{ba}\mp kv_z-\delta)^2/2v_x^2} \\ &\quad e^{i(\omega-\omega_{ba}\mp kv_z-\delta)(x_2-x_1)/v_x}a^{(0)}(p_z)a^{(0)*}(p_z) \end{aligned} \tag{11}$$

This Ramsey interference pattern has a blue recoil shift δ and is the superposition of fringe sub-systems corresponding to each velocity class, shifted by the first-order Doppler effect. If the transverse velocity distribution is too broad (absence of diaphragm) or in the optical domain, this will blur out the fringes. To make the connection with atom optics, this superposition can be rewritten as a correlation function involving the degree of coherence of the atom source [2]:

$$\int dz a^{(0)}(z \mp \frac{\hbar k}{M}(x_2 - x_1)/v_x, t)a^{(0)*}(z,t) \tag{12}$$

[2]The degree of transverse coherence of a thermal atom source is given by the density matrix element: $\langle z,t|\,\rho\,|z',t'\rangle$ which is simply the free propagator for a "complex time" argument: $t - t' - i\hbar/(k_B T)$. Its width is the thermal de Broglie wavelength h/Mu and it gives rise to the Doppler width $k_B u$. Incidentally, an accurate value for the Boltzman constant could be obtained through the accurate frequency measurement of a Doppler width.

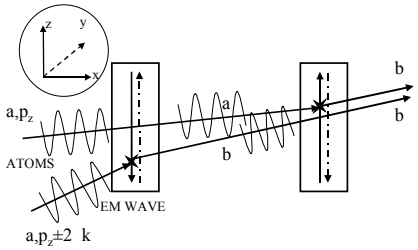

Figure 8. Illustration of the reinterpretation of the separated field method as the interference between de Broglie waves. Case of successive interactions with counterpropagating waves.

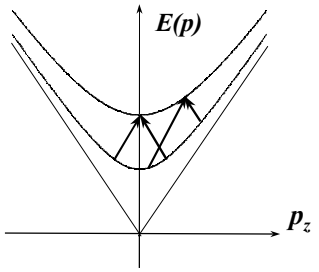

Figure 9. Energy vs transverse momentum exchanges in the case of successive interactions with counterpropagating waves.

Fringes will be obtained as long as $\hbar k\left(x_2-x_1\right)/Mv_x$ is smaller than the coherence width of the atom source. A second mechanism, which was considered only recently, is the interaction with oppositely travelling waves in each zone as in Figs 8 and 9.

This is possible only if the initial wave packet has Fourier components which differ by $\pm 2\hbar k$ (size of atomic cloud $< \lambda_{em}$) since:

$$\begin{aligned}\int dz b_{1\pm}^{(1)}(\overrightarrow{r},t)b_{2\mp}^{(1)*}(\overrightarrow{r},t) \quad &\propto \quad \int dz e^{\pm 2ikz}\int dp_z dp_z' \exp\left[i\left(p_z-p_z'\right)z/\hbar\right]... \\ ...a^{(0)}(p_z)a^{(0)*}(p_z') \quad &\Rightarrow \quad \delta\left(p_z-p_z'\pm 2\hbar k\right) \end{aligned} \tag{13}$$

The resulting signal exhibit fringes with an opposite recoil shift $-\delta$. Unlike the previous one, this signal depends upon the propagation characteristics

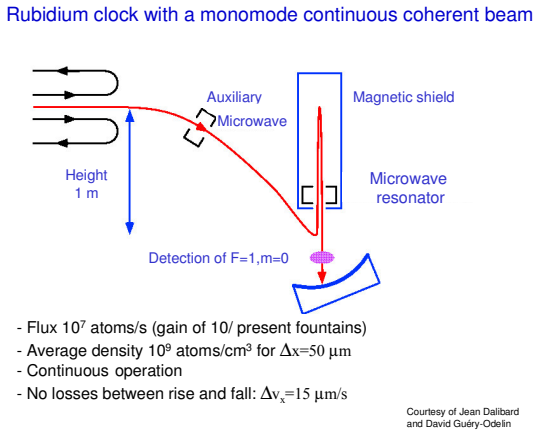

Figure 10. Schematic view of a possible future fountain clock using the continuous coherent atom wave source which is being developed at LKB (Paris). The magnetic mirror is in the strong field regime, in which four magnetic sublevels bounce upwards (including one connected with F=2, m=0), and the four others are attracted (including one connected with F=1, m=0). This guarantees a detection on a dark background.

of the incident atom wave:

$$\int dz b^{(1)}_{1\pm}(\overrightarrow{r},t) b^{(1)*}_{2\mp}(\overrightarrow{r},t) \quad \propto \quad e^{i(\omega-\omega_{ba}+\delta)(x_2-x_1)/v_x}$$
$$\cdot \int dp_z e^{-i(\pm kv_z+2\delta)(2x_0-x_2-x_1)/v_x} \qquad a^{(0)}(p_z)a^{(0)*}(p_z \pm 2\hbar k) \qquad (14)$$

This integral is easily calculated for Gaussian wave packets and statistical mixtures. If the waist position x_0 of the atom wave is not well-defined (e.g. in a thermal beam), energy conservation requires $kv_z = \mp 2\delta$ and will not be satisfied for most velocities (Fig. 9) and this signal will tend to average out. For a coherent atom wave, if the waist is located at x_1, this second contribution will have the same magnitude as the first one and the overall recoil shift will cancel [14]. If it is focussed at the midpoint $x_0 = (x_1+x_2)/2$ (perfect time reversal), this signal will be free of Doppler effect and will tend to dominate and impose its opposite recoil shift. This would be the case, for example, of a coherent atom wave with a waist at the top of a fountain clock, which could be achieved in a clock design such as that represented on Fig. 10.

4. Introduction of gravito-inertial fields

The well-known stationary solution of Schroedinger equation in presence of a gravitational field involving the Airy function can be applied directly to

the fountain clock. However, calculations with the Airy function are not so easy and here, we prefer to take a more general time-dependent approach, which is mathematically simpler and more powerful. To take gravito-inertial fields into account in the treatment of fountain clocks and other atom interferometers, we shall consider quite generally the non-relativistic Schroedinger equation obtained as the non-relativistic limit of a general relativistic equation described in the second part of this course:

$$\begin{aligned} i\hbar\frac{\partial|\Psi(t)\rangle}{\partial t} &= \Big[H_0 + \frac{1}{2M}\overrightarrow{p}_{op}.\overrightarrow{\overrightarrow{g}}(t)\cdot\overrightarrow{p}_{op} - \overrightarrow{\Omega}(t)\cdot(\overrightarrow{L}_{op}+\overrightarrow{S}_{op}) \\ &\quad -M\vec{g}(t)\cdot\vec{r}_{op} - \frac{M}{2}\vec{r}_{op}.\overrightarrow{\overrightarrow{\gamma}}(t)\cdot\vec{r}_{op} + V(\vec{r}_{op},t)\Big]|\Psi(t)\rangle \quad (15) \end{aligned}$$

where H_0 is an internal atomic Hamiltonian and $V(\vec{r}_{op},t)$ some general interaction Hamiltonian with an external field. Gravito-inertial fields are represented by the tensors $\overrightarrow{\overrightarrow{g}}(t)$ and $\overrightarrow{\overrightarrow{\gamma}}(t)$ and by the vectors $\overrightarrow{\Omega}(t)$ and $\vec{g}(t)$. The same terms can also be used to represent the effect of various external electromagnetic fields. The operators $\overrightarrow{L}_{op} = \vec{r}_{op}\times\overrightarrow{p}_{op}$ and $\overrightarrow{S}_{op}$ are respectively the orbital and spin angular momentum operators. Apart from in $V(\vec{r}_{op},t)$ we have limited the dependence of the Hamiltonian to second-order in the operators $\overrightarrow{p}_{op}$ and $\vec{r}_{op}$.

The rotation terms are easily removed with a unitary transformation, which rotates all quantities [3, 15]. The exact propagator of this equation in the absence of $V(\vec{r}_{op},t)$ has been derived by introducing a vector $\vec{\xi}$ such that[3]:

$$\overrightarrow{\ddot{\xi}} - \overrightarrow{\overrightarrow{\gamma}}(t)\cdot\vec{\xi} - \vec{g} = 0 \quad (16)$$

and the ABCD matrices of Gaussian optics[3, 15]. As an example, for one space dimension z, the following result (corrected from reference [2]) is obtained for the wave packet at (z,t) :

$$\begin{aligned} &\exp\left[\frac{iM}{\hbar}\dot{\xi}(z-\xi)\right]\exp\left[\frac{iM}{\hbar}\int_{t'}^{t}(\dot{\xi}^2/2+\gamma\xi^2/2-g\xi)dt_1\right] \\ &\int_{-\infty}^{+\infty}dz'\left(\frac{M}{2\pi i\hbar B}\right)^{1/2}\exp\left[(iM/2\hbar B)(D\,(z-\xi)^2-2\,(z-\xi)\,z'+Az'^2)\right] \\ &\exp\left[iMv_0(z'-z_0)/\hbar\right]F\left(z'-z_0,X_0,Y_0\right) \\ =\ &\exp\left[\frac{iS(t,t_0)}{\hbar}\right]\exp\left[\frac{iM}{\hbar}v(t)\,(z-z(t))\right]F(z-z(t),X(t),Y(t)) \quad (17) \end{aligned}$$

[3]For simplicity, we have left out the tensor $\overrightarrow{\overrightarrow{g}}(t)$ in what follows. This tensor is useful to represent the effect of gravitational waves. The reader interested in keeping this term is invited to use the more general equation derived in [3].

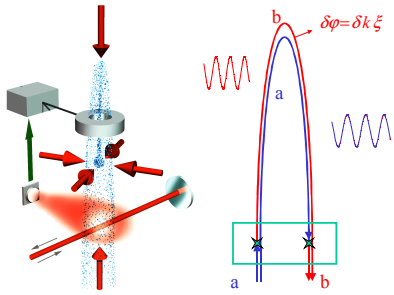

Figure 11. Phase shift in a fountain clock

$$\begin{aligned}\text{where } S(t,t_0) &= M\dot{\xi}(Az_0+Bv_0+\xi)-\frac{M}{2}\int_{t_0}^{t}(\dot{\xi}^2+\gamma\xi^2)dt_1\\ &\quad+\frac{M}{2}(ACz_0^2+DBv_0^2+2BCz_0v_0)\\ &= \frac{M}{\gamma^{3/2}}\left[\frac{g^2}{4}\left(\sinh 2x-2x\right)+\frac{\gamma}{4}\left(v_0^2-2gz_0+\gamma z_0^2\right)\sinh 2x\right.\\ &\quad\left.+\sqrt{\gamma}v_0\left(-g+\gamma z_0\right)\sinh^2 x\right] \qquad (18)\end{aligned}$$

is the classical action, with $x=\sqrt{\gamma}(t-t_0)$ and where

$$F\left(z-z_0,X_0,Y_0\right)=\frac{1}{\sqrt{X_0}}\exp\left[\frac{iM}{2\hbar}\frac{Y_0}{X_0}(z-z_0)^2\right] \qquad (19)$$

is a Gaussian (more generally Hermite-Gaussian) wave packet at the initial time t_0 in which the central position z_0, the initial velocity v_0 and the initial complex width parameters X_0, Y_0 in phase space, have to be replaced by their values at time t given by the $ABCD\xi$ transformation law:

$$\begin{aligned}z(t) &= Az_0+Bv_0+\xi \quad ; \quad X(t)=AX_0+BY_0\\ v(t) &= Cz_0+Dv_0+\dot{\xi} \quad ; \quad Y(t)=CX_0+DY_0 \qquad (20)\end{aligned}$$

In the limit where $\gamma\to 0$, $A=D\to 1$, $B\to t-t_0$, $C\to 0$, $\xi\to -(1/2)g(t-t_0)^2$ and $S\to M(t-t_0)\left(v_0^2-2gz_0-2gv_0(t-t_0)+2g^2(t-t_0)^2/3\right)/2$.

Let us apply this result to fountain clocks (Fig.11).

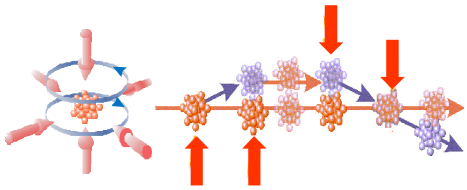

Figure 12. Magneto-optical trap (MOT on the left) and sequence of four laser beam spatial zones or time pulses to generate a closed atom interferometer in space or space-time (on the right).

We have seen that the total phase factor acquired by the atomic wave packet is: $\exp\left[\frac{iS(t,t_0)}{\hbar}\right]\exp\left[ip(t)\left(z-z(t)\right)/\hbar\right]$ [4]. On one arm the additional momentum communicated after the first interaction:

$$\hbar\delta k=\hbar\left(\omega-\omega_{ba}(v)\mp kv_z-\delta\right)/v_x$$

combined with $\xi=-(1/2)gT^2$, in the second phase factor, gives the phase shift responsible for the Ramsey fringes $\delta k\xi$. Note that this phase shift is indeed the same as in the atom gravimeter (see below) and an atom fountain clock is essentially a gravimeter with a recoil momentum communicated longitudinally proportional to the detuning. The phase factor which comes from the action gives the proper combination of gravitational phase shift and second-order Doppler effect (analogy with the Langevin twin paradox):

$$\left(S_b-S_a\right)/\hbar=-\omega_{ba}\left[1+\frac{1}{6}\frac{v_0^2}{c^2}\right]\left(\frac{2v_0}{g}\right) \tag{21}$$

5. Optical atomic clocks

In the optical domain, more interaction zones are necessary to close the interferometer[16, 17, 18] and cancel the transverse phase shift (see figure 12).

[4]Quite generally, the phase shift along each arm $\left(S\left(t,t_0\right)-\left[\vec{p}\left(t\right).\vec{r}\left(t\right)\right]_{t_0}^{t}\right)/\hbar$ is equal to minus the time integral of the kinetic energy.

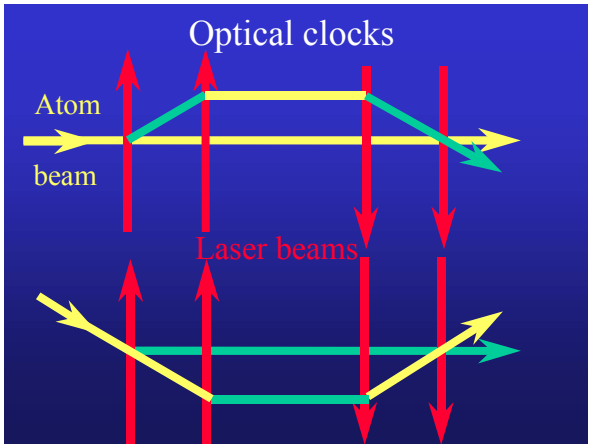

Figure 13. Pair of interferometers generated by two counterpropagating pairs of two copropagating laser beams. In one case the atoms are in their ground state in the central gap while they are in the excited state in the second interferometer central drift zone. The four interaction regions may be separated in space or in the time domain. They may involve single photon or multiphoton (Raman or cascade) transitions.

This closed circuit may have different shapes [18]: parallelogram (case of three or four copropagating laser beams) or trapezoid (two counterpropagating pairs of copropagating laser beams) or more complicated geometries with larger deviations [21, 19, 20]. The choice depends on the type of phase shift that one wishes to measure: symmetric configurations are sensitive only to inertial effects while asymmetric ones depend also on the laser detuning. A variety of transition processes and effective fields may be used: single photon, two-photon transitions of Raman or cascade type [17, 18]. These interactions may be separated in space to generate a spatial interferometer [10, 25] or in time to generate a space-time interferometer, as in recent realizations of optical clocks [9, 22, 23], which use magneto-optical traps of Ca, Sr or Mg. Cold atoms are released from a magneto-optical trap and submitted to the four pulses required to generate the interferometer. An interference pattern such as that displayed in Fig. 14 is obtained. High performances of stability and accuracy have been achieved in these various experiments.

In the case of the trapezoid geometry, there are two different interferometers created by two counterpropagating pairs of copropagating laser beams (Figure 15) with opposite recoil shifts. The two fringe systems are separated by 2δ. This splitting is clearly resolved on Fig. 16 where the velocity distribution in a thermal beam of Magnesium averages out the side fringes. In current realizations of optical clocks the fringe spacing is set precisely

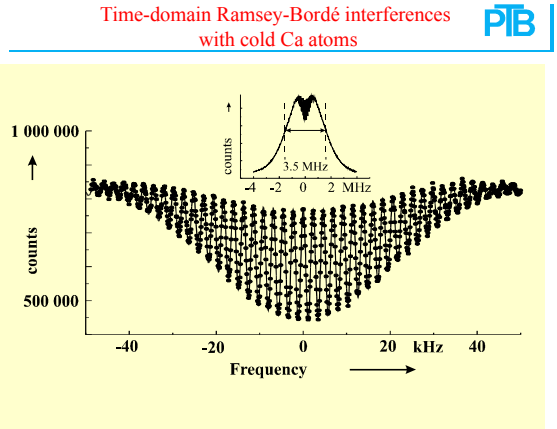

Figure 14. Interference pattern of an optical Calcium clock (*Courtesy of F. Riehle, P.T.B.*)

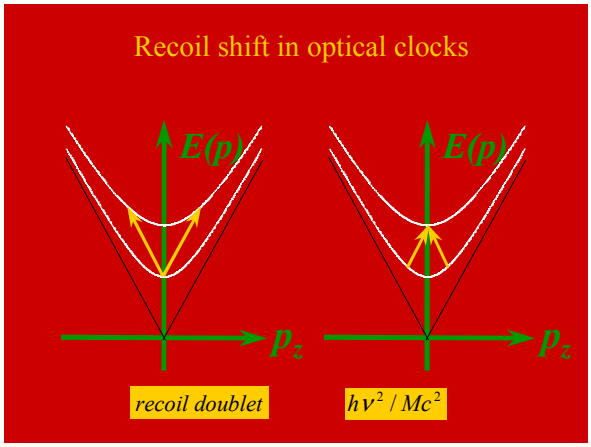

Figure 15. Energy-momentum diagrams illustrating exchanges in the two interferometers obtained with two counterpropagating pairs of two copropagating laser beams. The recoil shifts of central fringes are opposite. The first manifestation of this splitting was observed in the saturation spectrum of the methane molecule [24] and was the first quantitative demonstration of the exchange of momentum $\hbar k$ between light and an atomic species.

equal to this recoil splitting, in order to have two superimposed interference patterns as in Fig. 14.

In other experiments this recoil splitting is used to perform an accurate frequency measurement of $\hbar/m_{atom}$ and consequently of the fine structure

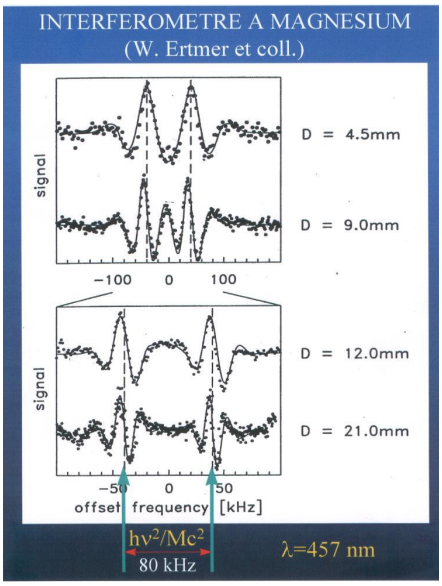

Figure 16. Interference patterns obtained with a Magnesium interferometer by the group of W. Ertmer [9]. Because of the thermal velocity distribution, only the central fringes dominate and one can see clearly the recoil splitting between the two fringe systems, with a resolution (reciprocal fringe width) increasing with the distance between the beam splitters.

constant α thanks to the relation:

$$\alpha^2 = \frac{2R_\infty}{c}\frac{m_p}{m_e}\frac{m_{atom}}{m_p}\frac{h}{m_{atom}}$$

where all quantities (Rydberg constant, ratio of proton mass m_p to the electron mass m_e ..) may be known with an accuracy equal or better than 10^{-9}, which means that α may be determined directly with an accuracy at the 10^{-9} level [20]. Since the recoil shift is proportional to the difference in kinetic energies in both arms of the interferometer, it can be increased very significantly (quadratically) by an accumulation of momentum quanta $\hbar k$ on one arm with respect to the other arm [21, 19, 20]. Recent determinations on Earth by the group of S. Chu have been pushed as far as the 10^{-8} level, which is of great importance as a test of QED, given the discrepancies between various other determinations and independently of any QED calculation.

The theory of optical clocks begins with perturbative and numerical approaches around 1977 [16]. A more sophisticated theory, which is still

used to describe experimental results, introduces 2x2 ABCD matrices in the internal spinor space of the two-level system and free propagation between pulses/field zones and was first published in 1982 [26, 27]. In 1990, the ABCDξ formalism for atom wave propagation in gravito-inertial fields has been presented, for the first time, in Les Houches [15]. The strong field S-matrix treatment of the electromagnetic field zones was then published in 1994 [13, 10]. In 1995, the problem of Rabi oscillations in a gravitational field has been treated in analogy/complementarity with the frequency chirp in curved wave-fronts [28]. Finally the dispersive properties of the group velocity of atom waves in strong e.m. fields have been described as a generalization of the dynamical neutron diffraction theory [30] in neutron beam splitters [29, 31, 32]. To-day we combine all these elements in a new sophisticated and realistic quantum description of optical clocks. This effort is also underway for atomic inertial sensors and is essential to develop strategies to eliminate the inertial field sensitivity of optical clocks [22]. In the next paragraphs, we outline the complete general relativistic derivation of phase shifts which was published in 1999 [4].

6. General relativistic framework for atom interferometry:

It is possible to include all possible effects of inertial fields, as well as all the general relativistic effects of gravitation in a consistent and synthetic framework[33, 29, 4], in which the atomic fields are second-quantized. The starting point is the use of coupled field equations for atomic fields of a given spin in curved space-time: e.g. coupled Klein-Gordon, Dirac or Proca equations. Gravitation is described by the metric tensor $g_{\mu\nu}$ and by tetrads, which enter in these equations. Several strategies can then be adopted: one can perform Foldy-Wouthuysen transformations [34], but conceptual difficulties arise in the case of arbitrary $g_{\mu\nu}$; one can go to the weak-field limit $g_{\mu\nu} = \eta_{\mu\nu} + h_{\mu\nu}$ with $|h_{\mu\nu}| \ll 1$ and use renormalized spinors and finally one can consider $h_{\mu\nu}$ as a spin-two tensor-field in flat space-time [36, 37, 38] and use ordinary relativistic quantum field theory. Using this last approach, it has been possible to derive field equations that display all interesting terms, coupling Dirac atomic fields, gravitational and electromagnetic fields and simple expressions of the corresponding relativistic phase shifts in atom interferometers [4].

The evolution equation of the state vector $|\Psi(t)\rangle$ in the interaction picture is

$$i\hbar \frac{d}{dt} |\Psi(t)\rangle = \int d^3x \ \theta^\dagger(x) \mathcal{V}_G(x) \theta(x) \ |\Psi(t)\rangle \,, \tag{22}$$

where the operator $\mathcal{V}_G(x)$, acting on the field operator $\theta(x)$, is given in

compact form by:

$$\mathcal{V}_G = \frac{c}{4}\alpha^\mu h_{\mu\nu} p^\nu + h.c. = \frac{c}{4}\left\{\alpha^\mu h_{\mu\nu}, p^\nu\right\}_+ \quad (23)$$

$$\text{with } p^0 = -\alpha^j p_j + \gamma^0 mc \text{ and } p_j = i\hbar\partial_j \quad (24)$$

The free field operator θ is written as:
$\theta(x) = \sum_{r=1}^{2}\int(d^3p)\left[c_r(\overrightarrow{p})\chi^{(+)}_{\overrightarrow{p},r}(x) + d^\dagger_r(\overrightarrow{p})\chi^{(-)}_{\overrightarrow{p},r}(x)\right]$, where $c_r(\overrightarrow{p})$ and $d_r(\overrightarrow{p})$ are the annihilation operators for the particles or antiparticles, respectively, and $\chi^{(\pm)}_{\overrightarrow{p},r}$ are the positive or negative energy solutions of the free Dirac equation:

$$\chi^{(\pm)}_{\overrightarrow{p},r}(x) = \frac{1}{(2\pi\hbar)^{3/2}}\sqrt{\frac{Mc^2}{E(\overrightarrow{p})}}u^{(r)}_{(\pm)}(\overrightarrow{p})e^{\mp i(E(\overrightarrow{p})t - \overrightarrow{p}.\overrightarrow{r})/\hbar} \quad (25)$$

We are interested in the output spinor corresponding to one-particle (antiparticle) states: e.g. $\psi(x) = \langle 0|\,\theta(x)\,|\Psi(t)\rangle$ for atoms. The evolution of this spinor is governed by the equation:

$$i\hbar\partial_t\psi = -i\hbar c\gamma^0\gamma^j\partial_j\psi + Mc^2\gamma^0\psi + \mathcal{V}_G(x)\psi \quad (26)$$

to which we may add terms corresponding to diagonal magnetic dipole and off-diagonal electric dipole interactions [33, 29]. This equation has been used in reference [29, 4] to discuss all the terms that lead to a phase shift in an interferometer.

For the phase shift, the general result is:

$$\begin{aligned}\delta\varphi = & -\frac{1}{\hbar}\int_{t_0}^{t}dt'\left\{\frac{c^2}{2E(\vec{p})}p^\mu h_{\mu\nu}(\vec{x}_0+\vec{v}t',t')p^\nu\right.\\ & +\frac{\gamma}{m(\gamma+1)}\left[\frac{c^2p^\mu\vec{\nabla}h_{\mu\nu}(\vec{x}_0+\vec{v}t',t')p^\nu}{2E^2(\vec{p})}\times\vec{p}\right]\cdot\overrightarrow{\overline{s}}\\ & \left.-\frac{c}{2}\left[\vec{\nabla}\times\left(\vec{h}(\vec{x}_0+\vec{v}t',t')-\overrightarrow{\overrightarrow{h}}\,(\vec{x}_0+\vec{v}t',t')\cdot\frac{\vec{p}c}{E(\vec{p})}\right)\right]\cdot\overrightarrow{\overline{s}}\right\} \quad (27)\end{aligned}$$

where $\overrightarrow{\overline{s}}$ is the mean spin vector

$$\overrightarrow{\overline{s}} = \sum_{r,r'}\beta^*_{r,i}\beta_{r',i}\hbar w^{(r)\dagger}\vec{a}w^{(r')}/2\gamma \quad (28)$$

where $\vec{a} = (\vec{\sigma}_\perp + \gamma\vec{\sigma}_\parallel)$ is the spatial part of the Thomas-Pauli-Lubanski 4-vector operator [39].

Expression (27) displays all the terms which may lead to a gravitational phase shift in a matter-wave interferometer:

- the terms involving h_{00} lead to the gravitational shift ($h_{00} = -2\ \vec{g}\cdot\vec{r}/c^2$), to shifts involving higher derivatives of the gravitational potential and to the analog of the Thomas precession (spin-orbit coupling corrected by the Thomas factor).
- the terms which involve $\vec{h} = \{h^{0k}\}$, give the Sagnac effect in a rotating frame ($\vec{h} = \vec{\Omega}\times\vec{\mathbf{r}}/c$), the spin-rotation coupling and a relativistic correction (analogous to the Thomas term for h_{00}). They describe also the Lense-Thirring effects coming from inertial frame-dragging by a massive rotating body, which is a source for $\vec{h}$.
- the other terms, which involve the tensor $\overrightarrow{\overrightarrow{h}} = \{h^{ij}\}$ describe genuine General Relativity effects such as the effect of gravitational waves and de Sitter geodetic precession (which also includes the Thomas term for h_{00}[5]).

In fact the phase calculation is usually more involved since formula (27) applies only to the case of straight unperturbed trajectories. In practice, however, one cannot ignore the fact that, when calculating the phase to first-order for a given term of the Hamiltonian, the motion of the particles is affected by other terms. One example, mentioned above, is the calculation of the gravitational shift within the atom beam splitters, in which one cannot ignore the important effects of the diffracting electromagnetic field on the trajectories of the particles [29, 31, 28, 32]. Gravitational phase shifts have to be calculated along these trajectories. Another example is the gravity field itself, which, on earth, gives parabolic trajectories for atoms. The phase shift for the other terms in equation (27) has to be calculated along these parabolas. A convenient way to achieve these calculations is to replace $\vec{x}_0 + \vec{v}t'$ and $\vec{v}$ in equation (27) by the classical trajectory $\{\vec{x}(t'), \vec{v}(t')\}$ obtained in the $ABCD$ formalism. In the non-relativistic limit, one is brought back to the Schroedinger equation and, up to second degree in position and momentum operators, the best approach is to take the full benefit of the $ABCD$ formalism developed above, which gives exact results. Higher-order terms can be treated as perturbations along unperturbed trajectories.

The reader will find calculations of the phases corresponding to the various terms in references [18, 17, 29, 40, 41]. In these calculations, one should never forget that the external field $h_{\mu\nu}$ acts not only on the atoms but also on other components of the experiments, such as mirrors and laser beams and that, depending on the chosen gauge, additional contributions may enter in the final expression of the phase which should, of course, be gauge independent. As an example, the Sagnac phase which can be removed

[5]Some authors reserve the name "Thomas precession" for the contribution coming specifically from an acceleration $\vec{a}$ (which has been included here in h_{00}) and separate it from de Sitter precession.

from the above formula by a simple coordinate transformation will reappear in the beam splitter phases.

The expressions valid for spins 0 and 1/2 may be conjectured to be valid for arbitrary spin if $\vec{\sigma}/2$ is replaced by the corresponding spin operator $\vec{S}$. The extension of the formulas is presently underway using higher spin formalisms.

Formula (27) also displays the analogy with electromagnetic interactions: $h_{\mu\nu}p^{\nu}/2$ plays the role of the 4-potential A_{μ} and $(E(\vec{p})/2c)\vec{\nabla}\times\left(\vec{h}-\overrightarrow{\overrightarrow{h}}\cdot\vec{p}c/E(\vec{p})\right)$ plays the role of a gravitomagnetic field $\vec{\nabla}\times\overrightarrow{A}$. This new correspondence between the gravitational interaction and the electromagnetic interaction generalizes the so-called gravitoelectric and gravitomagnetic interactions introduced by de Witt [42] and Papini [43].

The spin-independent part of this phase shift (Linet-Tourrenc [44] term) $\left(c^2/2E(\vec{p})\right)p_{\mu}h^{\mu\nu}p_{\nu}$, (combination which appears also in the generalized Thomas precession) corresponds to $u_{\mu}A^{\mu}/\gamma$ where u_{μ} is the 4-velocity p_{μ}/M and the corresponding circulation of potential takes the form of the Aharonov-Bohm phase formula $\oint A^{\mu}dx_{\mu}$. Using Stokes theorem in four dimensions, this integral gives the phase shift as the ratio of the flux of gravitoelectromagnetic forces through the interferometer space or spacetime area to a quantum of flux of force $\hbar$ or $\hbar c$:

$$\begin{aligned} -\hbar\delta\varphi &= \oint\frac{c^2}{2E(\vec{p})}p^{\mu}h_{\mu\nu}p^{\nu}dt=\oint\frac{1}{2}p^{\mu}h_{\mu\nu}dx^{\nu} \\ &= \frac{1}{2}\iint d\sigma^{\mu\nu}\left(\partial_{\mu}A_{\nu}-\partial_{\nu}A_{\mu}\right)\text{ with }A_{\nu}=\frac{1}{2}p^{\mu}h_{\mu\nu} \end{aligned} \tag{29}$$

in analogy with electromagnetism. This formula gives:

$$\delta\varphi=-\vec{k}.\vec{g}\;T^2 \tag{30}$$

for the gravitational phase shift[17, 18] as the flux of a gravitoelectric field $-c^2\vec{\nabla}h_{00}/2=\vec{g}$ through a space-time area (which is the case above for the fountain clock), whereas the Sagnac phase shift[6] is the flux of a gravitomagnetic field $c^2\vec{\nabla}\times\vec{h}=2c\vec{\Omega}$ through an area $\vec{A}$ in space [17, 18], which atomic clocks usually do not have:

$$\delta\varphi=\frac{2c\vec{\Omega}.\vec{A}}{\hbar c/M} \tag{31}$$

[6]This Sagnac phase shift (in units of 2π) can be written as the projection of the orbital angular momentum (in units of $\hbar$) of the interfering particles. An example of nuclear Sagnac interferometer is provided by rotating molecules, for which this phase shift is naturally quantized.

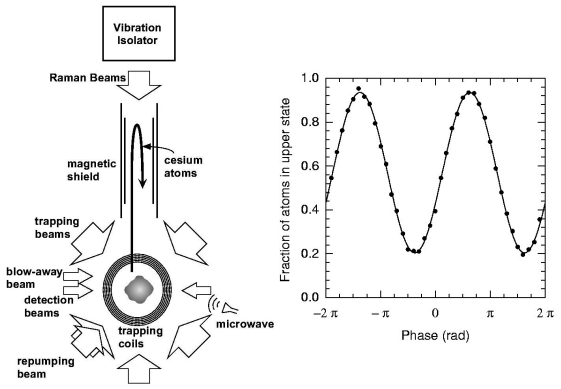

Figure 17. Atom-wave gravimeter developed at Stanford University by S. Chu and coworkers [47]. 5.10^8 Cesium atoms extracted from a low pressure background vapor are loaded in a MOT in 600 ms and launched upwards. A sequence of microwave, velocity sensitive Raman and state selective blow away pulses, places 3.10^6 atoms in the 6 $S_{1/2}$ F=3 $M_F = 0$ state with an effective vertical temperature of ~ 10 nK. The atomic cloud enters a magnetically shielded region and is illuminated by the sequence $\pi/2 - \pi - \pi/2$ of interferometer Raman pulses which enter from below. The retromirror is vibration isolated with an actively stabilized system. The right picture displays typical fringes for T=160 ms. Each point corresponds to a single launch of the atoms separated by 1.3 s and taken over one minute.

The spin-rotation term is discussed in more detail in references [29, 4]. Its effect on atomic clocks needs to be carefully evaluated, since, unlike the magnetic field, the gravitomagnetic field cannot be shielded.

7. State-of-the-art for gravito-inertial sensors

To emphasize the sensitivity of atom interferometers to inertial and gravitational fields, a short overview of realizations of gravito-inertial sensors, including gravimeters, gradiometers and atomic gyros is proposed to the reader in this last section. A first very successful application of atom interferometry is gravimetry and was developed by S. Chu and his collaborators (Fig. 17). This is an extension of the celebrated COW experiments for neutrons [45] to the atom world. In 1991, in one of the early experiments of atom interferometry [46], this group demonstrated a resolution of 3.10^{-8} for g in 40 minutes integration time. In recent earth gravity measurements, the relative sensitivity is $\delta g/g \simeq 3.10^{-9}$ after 60 seconds and the absolute accuracy 5.10^{-9}[20, 47]. This resolution is sufficient to see clearly the effect of ocean loading on the earth tides. Also, the agreement with a conventional

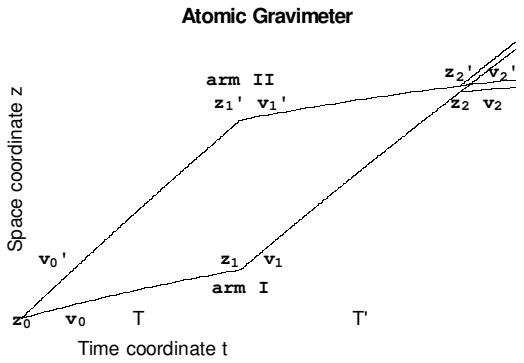

Figure 18. Space-time diagram of the atomic gravimeter.

corner cube gravimeter (FG-5) is at the $7.10^{-9}g$ level, which constitutes by itself, a test of the equivalence principle between an atomic species and a macroscopic object at that level. The corresponding space-time diagram is given in Fig.18. From which the following phase shift is calculated with the ABCDξ formalism [3]:

$$\begin{aligned}\delta\varphi &= -k((z_2+z_2')/2 - z_1 - z_1' + z_0) \\ &= -\frac{k}{\sqrt{\gamma}}\left[\left[\sinh\left(\sqrt{\gamma}(T+T')\right) - 2\sinh\left(\sqrt{\gamma}T\right)\right](v_0+\frac{\hbar k}{2M})\right. \\ &\quad \left.+\sqrt{\gamma}\left[1+\cosh\left(\sqrt{\gamma}(T+T')\right) - 2\cosh\left(\sqrt{\gamma}T\right)\right](z_0-\frac{g}{\gamma})\right] \quad (32)\end{aligned}$$

which, to first-order in γ and for $T = T'$ reduces to:

$$kgT^2 + k\gamma T^2\left[\frac{7}{12}gT^2 - (v_0+\frac{\hbar k}{2M})T - z_0\right] \quad (33)$$

where the first term, which is precisely expression (30), gives huge phase shifts for matter-waves compared to what could be obtained with light rays, since the times T can be of the order of one second, and gT^2 being of the order of ten meters is compared to an optical wavelength. The next term is a significant correction due to the gravitational field gradient γ. One can also measure directly these field gradients, with two gravimeters using two clouds of cold atoms and sharing the same vertical laser beam splitters. It is then no more necessary to have a very sophisticated inertial platform for the reference mirror and it is possible to measure directly

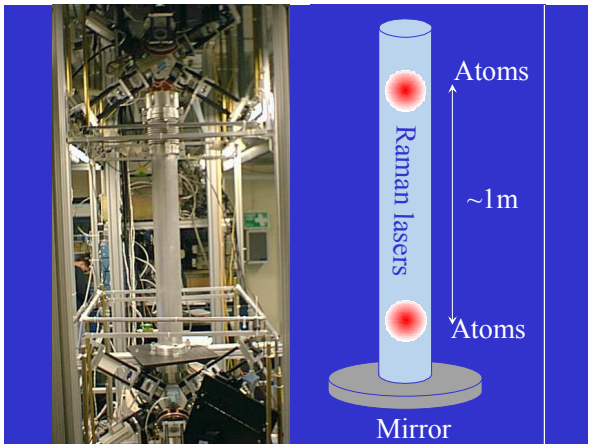

Figure 19. Atom wave gradiometer of Yale University. The two clouds of atoms share the same Raman beams, which generate two atom interferometers separated vertically by one meter.

the differential acceleration between these two clouds. This is the principle, illustrated in Fig.19, of the gradiometers developed first in Stanford then in Yale by M. Kasevich and his coworkers [20, 49]. The present sensitivity is $4.10^{-9}s^{-2}/\sqrt{Hz}$ or 4 E/$\sqrt{Hz}$ and the accuracy 1E/$\sqrt{Hz}$ for an extrapolated 10 m separation between accelerometers. For the future, one may think of using this principle for gravitational wave detection in space [48].

The first demonstration of a gyro using atom waves was performed at the P.T.B. in Braunschweig in a joint collaboration with the author [50]. The photograph of this experiment is given in Fig. 20. The Sagnac phase shift formula (31) given above reveals the considerable gain in sensitivity brought by matter-waves, since, in this formula, the rest mass energy Mc^2 has to be replaced by the photon energy $h\nu$ in the case of light waves. This expression can be derived by a number of equivalent approaches and the simplest one is to use the rotation operator in Schroedinger equation, which rotates the wave vectors of the beam splitters. This formula applies to the trapezoid geometry used in the previous experiment and also to the parallelogram geometry, as suggested in [18], analog of the Mach-Zehnder optical interferometer, which has been used in more recent experiments and which has the advantage of being insensitive to laser detuning. For rotations, the best sensitivity achieved up to now is 6.10^{-10}rad.s^{-1}Hz$^{-1/2}$ [51] with the set-up of Fig. 21. Clearly, if the atomic motion is reversed h_{00} is unchanged, while $\vec{h}.\vec{p}$ is reversed. This property is used to separate rotations and accelerations through the use of counterpropagating atomic

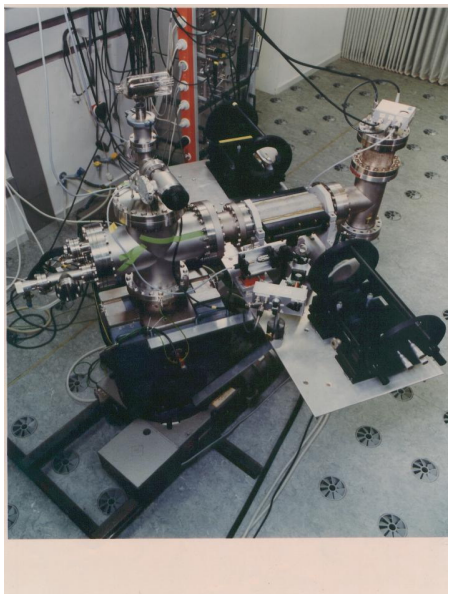

Figure 20. Photograph of the first atom wave gyro [50]. The calcium atomic beam originating from the oven on the left crosses two counterpropagating pairs of copropagating laser beams generated be the pair of cat's eyes facing each other on the right platform. These four beams act as beam splitters, deflectors and recombiner for the atom waves and the excited state output of the interferometer is monitored via the fluorescence light by the photomultiplier on the extreme right of the apparatus. The whole set-up is mounted on a rotating table.

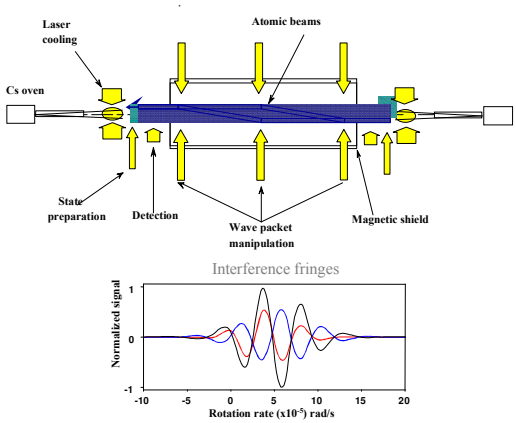

Figure 21. Atomic gyro developed at Yale in the group of Mark Kasevich. The Sagnac phases corresponding to the two opposite thermal atom beams have opposite signs and are substracted. The Earth rotation is responsible for the offset.

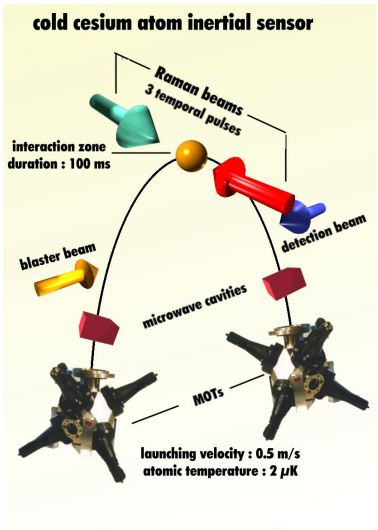

Figure 22. Principle of the cold Cesium gyro-accelerometer developed at the Observatory in Paris in collaboration between D. Holleville, J. Fils, A. Landragin, N. Dimarcq , A. Clairon (LHA and BNM-LPTF), Ph. Bouyer (IOTA), Ch. Salomon (LKB) and Ch. Bordé (LPL-ERGA).

beams. A compact device (30 cm height) using cold atoms and the Cesium clock technology (PHARAO) is under development in Paris, in a joint collaboration between several laboratories [52], and is shown in Figs.22 and 23. Here again, cold atoms are launched along counterpropagating parabolic trajectories, in order to separate the various components of the acceleration and of the rotation fields.

The sensitivity numbers quoted here are expected to improve rapidly in the near future, especially in space experiments, in which general relativistic effects should become detectable. The space project called HYPER [54] aims precisely at the detection of such effects thanks to the possibility to have long drift times in space (Fig.24). This will increase considerably the sensivity of these devices. The technology of trapping and manipulating cold atoms developed for the project ACES (Atomic Clock Ensemble in Space) will be directly applicable to inertial sensors for many applications in deep space navigation of space probes. Among the goals of HYPER, there is a very accurate measurement of the fine structure constant α, a test of the equivalence principle at the atomic level, using two different atomic species in the interferometer, a detection of the periodic signal coming from the latitudinal dependence of the Lense-Thirring effect in polar orbit, decoherence studies ....In fact, atom interferometers are so sensitive

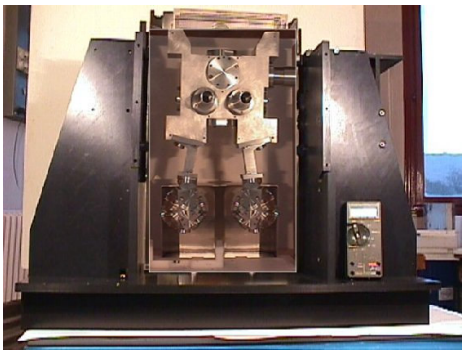

Figure 23. Cold atom gyro-accelerometer under construction at the Observatory in Paris.

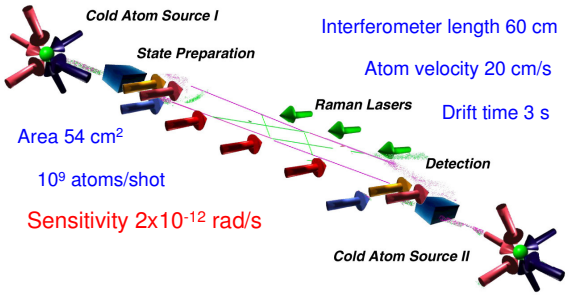

Figure 24. Schematic picture of an atom interferometer in space providing long drift times and a large interferometer area.

to gravito-inertial fields and to their gradients that, it will be necessary during the next years to develop many new techniques and tricks in the field of atom optics (e.g. phase conjugation of atom waves ...) to isolate the specific signature of investigated phenomena.

An accurate measurement of the effect of gravitation and inertia on antimatter also appears as a possibility already discussed in reference [53] with a transmission-grating interferometer, although we believe, for obvious reasons, that an antiatom interferometer using laser beams for the antihy-

drogen beam splitters (so-called Ramsey-Bordé interferometers) would be better suited for such an experiment. coherent beams of antihydrogen will be produced either by Bose-Einstein condensation and/or by stimulated bosonic amplification[7] [8].

References

1. *Atom Interferometry*, ed. P. Berman, Academic Press (1997).
2. Ch.J. Bordé, *Quantum theory of clocks and of gravitational sensors using atom interferometry, in:* Laser Spectroscopy, Eds. R. Blatt, J. Eschner, D. Leibfried and F. Schmidt-Kaler, World Scientific (1999) pp. 160-169.
3. Ch.J. Bordé, *Theoretical tools for atom optics and interferometry*, C.R. Acad. Sci. Paris, t.2, Série IV, 509-530 (2001).
4. Ch.J. Bordé, J.-C. Houard and A. Karasiewicz, *Relativistic phase shifts for Dirac particles interacting with weak gravitational fields in matter-wave interferometers*, in: Gyros, Clocks and Interferometers: Testing Relativistic Gravity in Space, Eds C. Lämmerzahl, C.W.F. Everitt and F.W. Hehl, Springer-Verlag, (2001) pp. 403-438 and gr-qc/0008033.
5. P. Lemonde et al., Cold atom clocks on earth and in space, in A.N. Luiten (Ed.), Frequency measurement and control, Topics Appl. Phys. **79**, 131-152 (2001). Springer-Verlag.
6. I. Bloch, T.W. Hänsch and T. Esslinger, *Measurement of the spatial coherence of a trapped Bose gas at the phase transition*, Nature **403**,166-170 (2000) and references therein.
7. I. Bloch, T.W. Hänsch and T. Esslinger, *Atom Laser with a cw Output Coupler*, Phys. Rev. Lett. **82**, 3008-3001 (1999).
8. Ch.J. Bordé, *Amplification of atomic fields by stimulated emission of atoms*, Physics Letters **A204**, 217-222 (1995); Ch.J. Bordé, *Amplification of atomic waves by stimulated emission of atoms*, in Laser Spectroscopy, edited by M. Inguscio, M. Allegrini and A. Sasso, World Scientific, 303-307 (1996); Ch.J. Bordé, *Amplification de champs atomiques par émission stimulée d'atomes*, Annales de Physique, **20**, 477-485 (1995).
9. U. Sterr, K. Sengstock, W. Ertmer, F. Riehle and J. Helmcke, *Atom interferometry based on separated light fields*, in [1].
10. Ch.J. Bordé, N. Courtier, F. du Burck, A.N. Goncharov and M. Gorlicki, *Molecular interferometry experiments*, Phys. Lett. A **188**, 187-197 (1994).
11. U. Sterr, K. Sengstock, J. H. Müller, D. Bettermann, W. Ertmer, *The magnesium Ramsey interferometer: applications and prospects*, Appl. Phys. B **54**, 341 (1992).
12. Ch.J. Bordé, J.L. Hall, C.V. Kunasz and D.G. Hummer, *Saturated absorption line shape: calculation of the transit-time broadening by a perturbation approach*, Phys. Rev. **14**, 236-263 (1976).

[7]using for example a reaction like: antiproton +positronium→antihydrogen+electron

13. J. Ishikawa, F. Riehle, J. Helmcke and Ch. J. Bordé, *Strong-field effects in coherent saturation spectroscopy of atomic beams,* Phys. Rev. **A49,** 4794-4825 (1994).
14. P. Wolf et al., *Recoil effects in microwave atomic frequency standards*, Proceedings of the 2001 IEEE Frequency Control Symposium, Seattle, USA, (2001), in press.
15. Ch. J. Bordé, *Propagation of Laser beams and of atomic systems*, Les Houches Lectures, Session LIII, 1990, *Fundamental Systems in Quantum Optics*, J. Dalibard, J.-M. Raimond and J. Zinn-Justin eds, Elsevier Science Publishers (1991) p.287-380.
16. Ch.J. Bordé, *Sur les franges de Ramsey en spectroscopie sans élargissement Doppler*, C. R. Acad. Sc. Paris, **284B**, 101-104 (1977), *Progress in understanding sub-Doppler line shapes*, in *Laser Spectroscopy III*, Springer-Verlag (1977).
17. Ch.J. Bordé, *Atomic interferometry with internal state labelling*, Phys. Lett., **A140**, 10-12 (1989).
18. Ch.J. Bordé, *Atomic interferometry and laser spectroscopy*, in: Laser Spectroscopy X, World Scientific (1991) pp. 239-245.
19. D.S.Weiss, B.C. Young and S. Chu, *Precision measurement of $\hbar/m_{Cs}$ based on photon recoil using laser-cooled atoms and atomic interferometry*, Applied Physics **B 59**, 217-256 (1994).
20. B.C. Young, M. Kasevich and S. Chu, *Precision atom interferometry with light pulses*, in [1] and references therein.
21. Ch.J. Bordé, M. Weitz and T.W. Hänsch, *New optical interferometers for precise measurements of recoil shifts. Application to atomic hydrogen*, in Laser Spectroscopy, L. Bloomfield, T. Gallagher and D. Larson eds, American Institute of Physics (1994) pp. 76-78.
22. T. Trebst, T. Binnewies, J. Helmcke and F. Riehle, *Suppression of spurious phase shifts in an optical frequency standard*, IEEE Trans. on Instr. and Meas. **50**, 535-538 (2001).
23. Th. Udem et al., *Absolute frequency measurements of the Hg^+ and Ca optical clock transitions with a femtosecond laser*, Phys. Rev. Lett. **86**, 4996 (2001).
24. J.L. Hall, Ch. J. Bordé and K. Uehara, *Direct optical resolution of the recoil effect using saturated absorption spectroscopy*, Phys. Rev. Lett. **37**, 1339 (1976).
25. Ch. J. Bordé, S. Avrillier, A. van Lerberghe, Ch. Salomon, Ch. Bréant, D. Bassi, and G. Scoles, *Observation of optical Ramsey fringes in the 10 μm spectral region using a supersonic beam of SF_6*, Appl. Phys. **B28**, 82 (1982) and Journal de Physique Colloques, **42**, C8-15-C8-19 (1981).
26. Ch.J. Bordé, *Développements récents en spectroscopie infrarouge à ultra-haute résolution*, Revue du Cethedec - Ondes et Signal, **NS83-1**, 1-118 (1983); Erratum n° 76, 191 (1983).
27. Ch. J. Bordé, Ch. Salomon, S. Avrillier, A. van Lerberghe, Ch. Bréant, D. Bassi, and G. Scoles, *Optical Ramsey fringes with traveling waves*, Phys. Rev. **A30**, 1836-1848 (1984).
28. C. Lämmerzahl and Ch.J. Bordé, *Rabi oscillations in gravitational fields: exact solution*, Physics Letters **A203**, 59-67 (1995).
29. Ch.J. Bordé, *Matter-wave interferometers: a synthetic approach*, in [1].
30. H. Rauch and D. Petrascheck, *Dynamical Neutron Diffraction*

and its Application, in Neutron Diffraction, ed. by H. Dachs (Springer, Berlin, 1978) pp. 303-351 and references therein.
31. Ch.J. Bordé and C. Lämmerzahl, *Atom beam interferometry as two-level particle scattering by a periodic potential*, Ann. Physik (Leipzig) **8**, 83-110 (1999).
32. C. Lämmerzahl and Ch.J. Bordé, *Atom interferometry in gravitational fields: influence of gravitation on the beam splitter*, General Relativity and Gravitation, **31**, 635 (1999).
33. Ch.J. Bordé, A. Karasiewicz and Ph. Tourrenc, *General relativistic framework for atomic interferometry*, Int. J. of Mod. Phys.**D 3**, 157-161 (1994).
34. F.W. Hehl and Wei-Tou Ni, *Inertial effects of a Dirac particle*, Phys Rev. **D 42**, 2045-2048 (1990).
35. K.-P. Marzlin and J. Audretsch, Phys.Rev. A**53**, 1004 (1996).
36. S.N. Gupta, *Quantization of Einstein's gravitational field: linear approximation*, Proc. Phys. Soc. **A 65**, 161-169 (1952) and *Quantization of Einstein's gravitational field: general treatment,* Proc. Phys. Soc. **A 65**, 608-619 (1952).
37. R.P. Feynman, F.B. Morinigo and W.G. Wagner, *Feynman Lectures on Gravitation,* edited by B. Hatfield (Addison-Wesley, Reading MA 1995).
38. B.M. Barker, S.N. Gupta and R.D. Haracz, *One-graviton exchange interaction of elementary particles*, Phys. Rev. **149**, 1027 (1966) and references therein.
39. L.H. Thomas, *The Kinematics of an Electron with an Axis*, Phil. Mag. **3**, 1-22 (1927).
40. J. Audretsch and K.-P. Marzlin, *Atom interferometry with arbitrary laser configurations: exact phase shift for potentials including inertia and gravitation*, J. Phys. II France **4**, 2073-2087 (1994).
41. J. Audretsch and K.-P. Marzlin, *Ramsey fringes in atomic interferometry: measurability of the influence of space-time curvature*, Phys. Rev. **A 50**, 2080 (1994).
42. B.S. DeWitt, *Superconductors and gravitational drag*, Phys. Rev. Lett. **16**, 1092 (1966).
43. G. Papini, *Particle wave functions in weak gravitational fields*, Nuovo Cimento **52B**, 136-140 (1967).
44. B. Linet et P. Tourrenc, *Changement de phase dans un champ de gravitation: possibilité de détection interférentielle*, Can. J. Phys. **54**, 1129-1133 (1976).
45. R. Collela, A.W. Overhauser and S.A.Werner, *Observation of Gravitationally Induced Quantum Interference*, Phys. Rev. Lett. **34,** 1472 (1975).
46. M. Kasevich and S. Chu, *Atomic interferometry using stimulated Raman transitions*, Phys. Rev. Lett. **67**, 181-184 (1991).
47. A. Peters, K. Y. Chung and S. Chu, *A measurement of gravitational acceleration by dropping atoms*, Nature **400**, 849 (1999) and *High precision gravity measurements using atom interferometry*, Metrologia **38**, 25-61 (2001).
48. For an early treatment of a gravitational wave detector using an atom interferometric gradiometer see: Ch.J. Bordé, J. Sharma, Ph. Tourrenc and Th. Damour, *Theoretical approaches to laser spectroscopy in the presence of gravitational fields*, J. Physique Lettres **44**, L-983-990 (1983).
49. M.J. Snadden, J.M. McGuirk, P. Bouyer, K.G. Haritos and

M.A. Kasevich, *Measurement of the Earth's gravity gradient with an atom interferometer-based gravity gradiometer*, Phys. Rev. Lett. **81**, 971-974 (1998).

50. F. Riehle, Th. Kisters, A. Witte, J. Helmcke and Ch.J. Bordé, *Optical Ramsey Spectroscopy in a Rotating Frame: Sagnac Effect in a Matter-Wave Interferometer,* Phys. Rev. Lett. **67**, 177-180 (1991).
51. A. Landragin, T. L. Gustavson and M. A. Kasevich, *Precision atomic gyroscope*, in Laser Spectroscopy, Proceedings of the 14th International Conference on Laser Spectroscopy, Eds. R. Blatt, J. Eschner, D. Leibfried and F. Schmidt-Kaler, World Scientific, Singapore (1999) pp. 170-176.
52. D. Holleville, J. Fils, P. Petit, N. Dimarcq, A. Clairon, P. Bouyer, Ch. Bordé et Ch. Salomon, *Réalisation d'un gyromètre à atomes froids*, J. Phys IV (France) **10**, Pr8-171 (2000).
53. T.J. Phillips, *Measuring the gravitational acceleration of antimatter with an antihydrogen interferometer*, Hyperfine Interactions **100**, 163-172 (1996).
54. R. Bingham et al., HYPER, *Hyper-Precision Cold Atom Interferometry in Space*, Assessment Study Report, ESA-SCI (2000) 10.